



This is a repository copy of *Influence of DC winding configuration on its induced voltage in wound field machines*.

White Rose Research Online URL for this paper:
<http://eprints.whiterose.ac.uk/139344/>

Version: Accepted Version

Article:

Wu, Z.Z., Zhu, Z.Q. orcid.org/0000-0001-7175-3307, Wang, C. et al. (3 more authors) (2018) Influence of DC winding configuration on its induced voltage in wound field machines. *IEEE Transactions on Energy Conversion*, 33 (4). pp. 1825-1836. ISSN 0885-8969

<https://doi.org/10.1109/TEC.2018.2846567>

© 2018 IEEE. Personal use of this material is permitted. Permission from IEEE must be obtained for all other users, including reprinting/ republishing this material for advertising or promotional purposes, creating new collective works for resale or redistribution to servers or lists, or reuse of any copyrighted components of this work in other works. Reproduced in accordance with the publisher's self-archiving policy.

Reuse

Items deposited in White Rose Research Online are protected by copyright, with all rights reserved unless indicated otherwise. They may be downloaded and/or printed for private study, or other acts as permitted by national copyright laws. The publisher or other rights holders may allow further reproduction and re-use of the full text version. This is indicated by the licence information on the White Rose Research Online record for the item.

Takedown

If you consider content in White Rose Research Online to be in breach of UK law, please notify us by emailing eprints@whiterose.ac.uk including the URL of the record and the reason for the withdrawal request.



eprints@whiterose.ac.uk
<https://eprints.whiterose.ac.uk/>

Influence of DC Winding Configuration on Its Induced Voltage in Wound Field Machines

Z. Z. Wu, Member, IEEE, Z. Q. Zhu, Fellow, IEEE, C. Wang, J. C. Mipo, S. Personnaz, and P. Farah

Abstract— DC winding induced voltage pulsation in the wound field synchronous machines (WFSMs) will cause DC winding current ripple, challenge the DC power supply and deteriorate the control performance, especially at high speed. In this paper, the influence of DC winding configuration including the DC coil number and the parallel branch number on its induced voltage pulsation is investigated for WFSMs. Based on the modelling of both open-circuit and on-load DC winding induced voltages, the preferred DC winding configurations for WFSMs having various stator / rotor pole number combinations with double layer or single layer AC windings are obtained and validated by finite element (FE) analysis on four typical partitioned stator WFSMs (PS-WFSMs). A PS-WFSM prototype is built and tested to validate both analytical and FE analyses.

Index Terms— DC coil number, DC winding configuration, DC winding induced voltage, DC winding parallel branch number, DC winding resistance voltage drop, on-load, open-circuit.

I. INTRODUCTION

PERMANENT MAGNET (PM) machines have been used for various applications due to the high torque / power density and efficiency [1], [2]. However, wound field synchronous machines (WFSMs) may potentially replace the PM machines to reduce the rare earth PM cost and improve the limited flux-weakening performance in PM machines [3]. The conventional wound-rotor machines having DC winding in the rotor but AC windings in the stator suffer from brushes and slip rings [4], which can be eliminated in the wound-stator machines [5]-[14]. In wound-stator machines, both the DC winding and AC windings are placed in the stator, whilst the salient rotor is simple without any DC coil or AC coil, similar to that of the switched reluctance machines [15], [16].

Wound field switched flux machine [6]-[14] is a typical type of wound-stator machine. When the salient pole rotor is rotating together with the stator DC field excitation, bipolar flux-linkage and hence back-EMF can be generated in the AC coils and hence AC windings. Therefore, the electromagnetic torque can be produced by injecting bipolar currents into AC windings [6]. Wound field switched flux machines for automotive propulsion and traction applications are analyzed in [11]-[14]. The experimental results show that the wound field switched flux machines can produce similar torque and power density as the PM machines but cost less.

To further improve the torque and power density, the DC winding and AC windings in the conventional wound field switched flux machines analyzed in [6] are separately placed in two stators to form the partitioned stator wound field synchronous machine (PS-WFSM) [17]. As shown in Fig. 1(a) for the 12/10-pole PS-WFSM having double-layer AC windings, the PS-WFSM has two stators, i.e. the outer stator and the inner stator wound by AC windings and DC winding, respectively, and one rotor consisting of several rotor iron pieces. Similar to the conventional wound field switched flux machine having single stator [6], the electromagnetic torque can be produced by injecting bipolar currents and DC currents into the AC windings and DC winding, respectively. As analyzed in [17], the PS-WFSM can produce more than 19% higher torque than its single stator counterpart with same size, due to higher utilization of the machine inner space.

Although the WFSMs have been researched for many years, however, the DC winding configuration has not been well investigated. The DC winding configuration consists of two aspects, i.e. the DC coil number N_w and the parallel branch number b . Normally, the DC coil number N_w is configured equal to the stator pole number N_s , i.e. $N_w=N_s$. However, as mentioned in [6], it was well recognized that the DC coil number N_w can also be designed as half of the stator pole number N_s , i.e. $N_w=N_s/2$, from the perspective of the same magnetic field and hence electromagnetic torque when the end-effect and end winding are neglected. Meanwhile, the DC coil number of turns N_c is doubled as $2N_c$ to form the same wound field MMF per pole F_w with the same DC winding current I_w and the same DC coil slot packing factor k_{pf} . As for the parallel branch number b , theoretically it was assumed to be free to design as long as the same wound field MMF per pole F_w obtained. In this paper, it will be shown that the DC winding configuration design in WFSMs is restricted due to the DC winding induced voltage pulsation.

DC winding induced voltage pulsation is due to the variation of the DC winding flux-linkage, which is caused by both the self-inductance of DC winding and the mutual inductance between AC and DC windings, as analyzed in [8] for the single phase WFSM. DC winding induced voltage will cause the DC winding current ripple [8], [9], challenge the DC power supply and deteriorate the control performance, especially at high speed. The aim of this paper is to provide the feasible and preferred DC winding configurations for WFSMs having various N_s/N_r -stator/rotor-pole combinations with double layer or single layer AC windings, for achieving a small DC winding induced voltage.

This paper is organized as follows. In section II, the influence of DC winding configuration on its resistance voltage drop is analyzed, whilst those on its open-circuit and on-load induced voltages are modelled and investigated in sections III and IV, respectively. Analytical analysis is validated by finite element (FE) simulation in section V. A PS-WFSM prototype is built and tested to validate both the analytical and FE results in section VI. Then, the impact of

Manuscript received December 1, 2017; revised March 26, 2018 and May 22, 2018; accepted June 9, 2018. Paper no. TEC-00920-2017. (Corresponding Author: Z. Q. Zhu.)

Z. Z. Wu, Z. Q. Zhu, and C. Wang are with the Electrical Machines and Drives Group, University of Sheffield, Sheffield, UK (wuzhongze@gmail.com, z.q.zhu@sheffield.ac.uk, cwang55@sheffield.ac.uk).

J. C. Mipo, S. Personnaz, and P. Farah are with Valeo Powertrain Electric Systems, 94017 Créteil Cedex, France (jean-claude.mipo@valeo.com, sophie.personnaz@valeo.com, philippe.farah@valeo.com).

DC winding induced voltage is analyzed in section VII, followed by conclusion in section VIII.

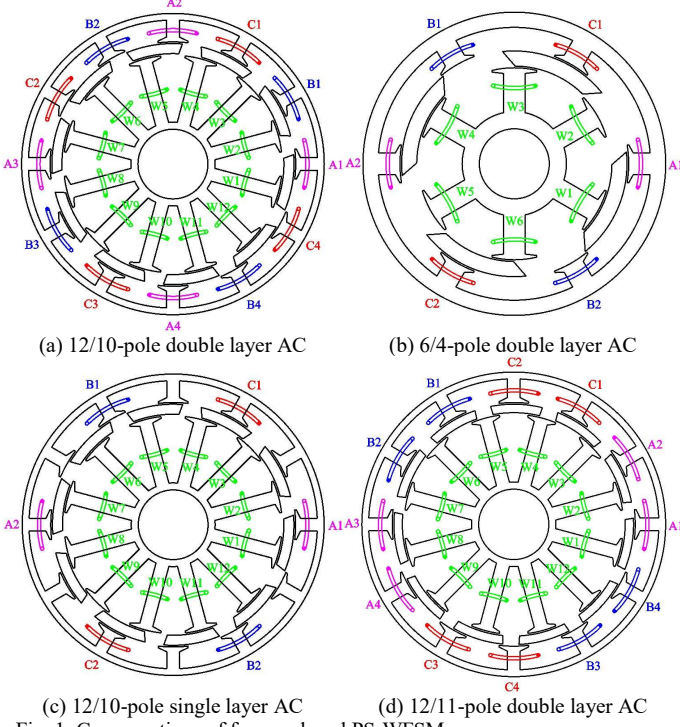


Fig. 1. Cross-sections of four analyzed PS-WFSMs.

II. DC WINDING RESISTANCE VOLTAGE DROP

When the end winding is neglected, the DC winding resistance R_w can be given by,

$$R_w = \frac{2N_w \rho l_s N_c^2}{b^2 A_s k_{pf}} \quad (1)$$

where N_w is the DC coil number. ρ is the copper resistance ratio. l_s is the stack length. N_c is the DC coil number of turns. b is the parallel branch number. A_s is the DC coil slot area. k_{pf} is the DC coil slot packing factor.

From the perspective of electric circuit, based on the Ohm's law, the DC winding resistance voltage drop U_w and the DC winding current I_w match,

$$U_w = I_w R_w \quad (2)$$

From the perspective of magnetic circuit, the wound field MMF per pole F_w can be expressed as,

$$F_w = \frac{I_w N_c N_w}{b N_s} \quad (3)$$

where N_s is the stator pole number.

Based on (1)-(3), with the DC winding current I_w eliminated, the DC winding resistance voltage drop U_w can be rewritten as,

$$U_w = \frac{2\rho l_s N_s}{k_{pf}} \times F_w \times \frac{N_c}{A_s b} \quad (4)$$

Based on (4), it can be found that the DC power supply voltage will be set as U_w to generate F_w in the magnetic circuit.

A. Influence of DC Coil Number N_w

As for machine having $N_w = N_s/2$, the DC coil slot area A_s is doubled, compared with that having $N_w = N_s$. Moreover, the DC coil number of turns N_c is also doubled to form the same wound field MMF per pole F_w with the same DC winding current I_w and the same DC coil slot packing factor k_{pf} . Therefore, as shown in (4), the DC winding resistance voltage drop U_w is the same in the WFSM having $N_w = N_s/2$ and $N_w = N_s$.

Here, according to (5), it is worth noting that the DC winding copper loss p_w is also the same with different N_w when F_w remains unchanged, since $A_s N_w$ is the same. Consequently, the electromagnetic performance, including electromagnetic torque, the loss and efficiency, is the same for a WFSM when the number of coils N_w is changed.

$$p_w = U_w I_w = \frac{2\rho l_s N_s^2}{k_{pf}} \times F_w^2 \times \frac{1}{A_s N_w} \quad (5)$$

B. Influence of Parallel Branch Number b

As shown in (4), the DC winding resistance voltage drop U_w is inversely proportional to the parallel branch number b , i.e. b could be a design variable to increase or reduce the DC winding resistance voltage drop U_w .

III. OPEN-CIRCUIT DC WINDING INDUCED VOLTAGE

In this section, the open-circuit DC winding induced voltage will be analytically modelled to investigate the influence of DC winding configuration, including the harmonics orders, harmonics amplitudes and the ratio of its peak-to-peak value to the DC winding resistance voltage drop U_w , as given as follows.

As derived in Appendix A, the open-circuit DC winding induced voltage v_{open} can be given as,

$$v_{open}(\theta_e) = \sum_{j=m}^{\frac{LCM(N_w, N_r)}{N_r}} A_{openj} \sin(j\theta_e + \gamma_{openj}) \quad (6)$$

where LCM is the least common multiplier and $m=1,2,3\dots$. A_{openj} and γ_{openj} are the corresponding amplitudes and initial phases for the v_{open} j^{th} harmonic in (A.13) in Appendix A, i.e.

$$A_{openj} = \frac{N_w N_c M_j \Omega}{b} \quad (7)$$

and

$$\gamma_{openj} = \frac{j\pi N_r}{N_w} + \alpha_j - j\pi N_r \quad (8)$$

Here, $N_c M_j \Omega$ and α_j are the amplitude and initial phase for the j^{th} harmonic of the open-circuit induced voltage for the DC coil W_1 , respectively. θ_e is the rotor electric position. M_j is the j^{th} amplitude of the open-circuit induced voltage for each turn in the DC coil per rotor mechanical speed unit. It is worth noting that M_j and α_j are the same in a certain WFSM with same magnetic field having different DC winding configurations. Ω is the rotor mechanical speed. N_r is the rotor pole number.

To comparatively evaluate the challenge of open-circuit DC winding induced voltage on the DC power supply and control performance deterioration, the open-circuit DC winding induced voltage ratio IVR_{open} is introduced, which is defined as the ratio of the peak-to-peak value of the open-circuit DC winding induced voltage E_{ppopen} in (6) to U_w in (4),

$$IVR_{open} = \frac{E_{ppopen}}{U_w} = \frac{\max(v_{open}) - \min(v_{open})}{U_w} = \frac{\max \left[\sum_{j=m}^{\frac{LCM(N_w, N_r)}{N_r}} Ripp_{openj} \sin(j\theta_e + \gamma_j) \right] - \min \left[\sum_{j=m}^{\frac{LCM(N_w, N_r)}{N_r}} Ripp_{openj} \sin(j\theta_e + \gamma_j) \right]}{U_w} \quad (9)$$

where $Ripp_{openj}$ is the j^{th} ripple of open-circuit DC winding induced voltage, which is defined as the j^{th} amplitude A_{openj}

in (7) to the DC winding resistance voltage drop U_w in (4),

$$Ripp_{openj} = \frac{A_{openj}}{U_w} = \frac{M_j}{2} \times \frac{k_{pf}}{\rho l_s N_s} \times \frac{1}{F_w} \times \Omega \times A_s N_w \quad (10)$$

A. Influence of DC Coil Number N_w

When $LCM(N_s, N_r) \neq LCM(N_s/2, N_r)$, as shown in (A.13) in Appendix A, v_{open} harmonic content is different for $N_w=N_s$ and $N_w=N_s/2$. v_{open} harmonic orders in the WFSM having $N_w=N_s/2$ are $mLCM(N_s/2, N_r)/N_r$, whilst those in PS-WFSM having $N_w=N_s$ are $2mLCM(N_s/2, N_r)/N_r$. As shown in (10), since $A_s N_w$ is the same in the WFSM having $N_w=N_s$ and $N_w=N_s/2$, $Ripp_{openj}$ is the same for the same harmonic orders, i.e. $2mLCM(N_s/2, N_r)/N_r$. However, the PS-WFSM having $N_w=N_s/2$ also suffers from v_{open} harmonics with $(2m-1)LCM(N_s/2, N_r)/N_r$ -pole-pair. Therefore, it has a larger IVR_{open} . This means v_{open} in the WFSM having $N_w=N_s/2$ challenges the DC power supply more and deteriorates the control performance more, especially at high rotor mechanical speed since $Ripp_{openj}$ and hence IVR_{open} are proportional to the rotor mechanical speed Ω , as shown in (10), whilst U_w is not relevant to Ω .

When $LCM(N_s, N_r) = LCM(N_s/2, N_r)$, however, v_{open} harmonic orders in (A.13) in Appendix A and amplitudes in (7) will be the same for the N_s/N_r -pole WFSM having $N_w=N_s$ and $N_w=N_s/2$. The corresponding $Ripp_j$ in (10) and IVR_{open} in (9) are also the same, since the DC winding resistance voltage drop U_w is the same for PS-WFSM having $N_w=N_s$ and $N_w=N_s/2$, as shown in (4). This means there is no influence for the DC coil number N_w on the open-circuit DC winding induced voltage v_{open} in this type of WFSMs, e.g. some $N_r=N_s \pm 2$ machines, including 6/4- and 6/8-stator/rotor-pole PS-WFSMs.

B. Influence of Parallel Branch Number b

Due to the DC coil induced voltages, it is found that the parallel branch number b is not free to design. If the DC coils connected in parallel have different open-circuit induced voltages, circulating current will be yielded among them. The circulating current will increase the copper loss by interacting with the coil resistance and the machine efficiency will be reduced. Therefore, the DC coils connected in parallel should have exactly the same open-circuit induced voltage.

As shown in (A.1) in Appendix A, $v_{k,open} = v_{k',open}$ (k and $k' = 1, 2, 3 \dots N_w$) when $\beta_k = \beta_{k'} + 2m\pi$ ($m = 0, \pm 1, \pm 2, \pm 3 \dots$), i.e. the difference Δk matches,

$$\Delta k = \frac{LCM(N_w, N_r)}{N_r} \quad (11)$$

As shown in (11), DC coils W_k and $W_{k+\Delta k}$ have the same open-circuit induced voltage, i.e. they can be connected in parallel without circulating current. Therefore, the maximum parallel branch number b_{max} can be achieved as,

$$b_{max} = \frac{N_r}{\Delta k} = \frac{N_w N_r}{LCM(N_w, N_r)} \quad (12)$$

It should be noted that b should be designed as a divisor of b_{max} , to achieve a symmetrical magnetic field. Specifically, when $b = b_{max}$, the open-circuit DC winding induced voltage v_{open} will be the minimum. Based on (6) and (12), the minimum available DC winding induced voltage $v_{openmin}$ is,

$$v_{openmin}(\theta_e) = \frac{LCM(N_w, N_r)}{N_w N_r} \sum_{j=m \frac{LCM(N_w, N_r)}{N_r}} A_{openj} \sin(j\theta_e + \gamma_j) \quad (13)$$

However, as shown in (4), U_w is also inversely proportional to b . Consequently, as shown in (9) and (10), $Ripp_{openj}$ and hence IVR_{open} is not relevant to b . Therefore, by changing the parallel branch number b to another feasible value, the control performance will remain the same.

IV. ON-LOAD DC WINDING INDUCED VOLTAGE

Under on-load condition, the DC winding flux-linkage and hence the induced voltage consists of two parts, i.e. open-circuit one and armature reaction one. The latter one is due to the interaction between AC currents and the mutual-inductance between the AC windings and the DC winding [8], [9]. The on-load DC winding induced voltage v_{load} can be expressed as,

$$v_{load} = v_{open} + v_{arma} \quad (14)$$

where v_{arma} is the DC winding induced voltage caused by armature reaction.

According to the derivation in Appendix B, the DC winding voltage induced by armature reaction v_{arma} can be rewritten as,

$$v_{arma}(\theta_e) = \frac{3I_1 N_w N_c N_r \Omega}{2b} \sum_{j=1}^{\infty} k_j M_j \times \begin{cases} -(j-1) \sin[(j-1)\theta_e + \delta_j - \sigma_1], & \text{for } j = 1, 4, 7 \dots \\ -(j+1) \sin[(j+1)\theta_e + \delta_j + \sigma_1], & \text{for } j = 2, 5, 8 \dots \\ 0, & \text{for } j = 3, 6, 9 \dots \end{cases} \quad (15)$$

where I_1 is the phase current fundamental amplitude. $k_j M_j$ and δ_j are the amplitude and initial phase of the j^{th} mutual-inductance harmonic. k_j is the j^{th} harmonic winding factor. σ_1 is the initial phase angle of phase A sinusoidal current.

Therefore, based on (14), v_{load} can be obtained by adding v_{open} in (6) and v_{arma} in (15). As shown in (15), armature reaction generates $3m^{\text{th}}$ ($m=1, 2, 3 \dots$) ψ_{arma} harmonics and hence induced voltage harmonics in the DC winding. However, when the winding factors of even order harmonics are zero, they are $6m^{\text{th}}$ ($m=1, 2, 3 \dots$). Moreover, the influences of N_w and b on v_{arma} and v_{load} are similar to those on the open-circuit one.

In some PS-WFSMs, the harmonic orders of the open-circuit and armature reaction induced DC winding voltage are same, e.g. $6m^{\text{th}}$ ($m=1, 2, 3 \dots$) for both the open-circuit DC winding induced voltage v_{open} and the armature reaction DC winding induced voltage v_{arma} in the 12/10-pole PS-WFSM with double layer AC windings. Therefore, the on-load DC winding induced voltage v_{load} is also with $6m^{\text{th}}$ harmonics. However, harmonic orders of v_{open} and v_{arma} may be different in some other PS-WFSMs, e.g. $12m^{\text{th}}$ and $6m^{\text{th}}$ ($m=1, 2, 3 \dots$) in the 12/11-pole PS-WFSM with double layer windings, respectively. Consequently, the on-load DC winding induced voltage v_{load} is with $6m^{\text{th}}$ harmonics, different from the open-circuit DC winding induced voltage v_{open} .

V. FE ANALYSIS

To verify the analytical analysis in the previous two sections, four typical PS-WFSMs are analyzed by FE analysis in this section. Firstly, to evaluate the influence of the DC winding configuration on the open-circuit DC winding induced voltage v_{open} , two PS-WFSMs are analyzed with $LCM(N_s, N_r) \neq LCM(N_s/2, N_r)$ and $LCM(N_s, N_r) = LCM(N_s/2, N_r)$, respectively, i.e. 12/10- and 6/4-pole PS-WFSMs with double layer AC windings shown in Fig. 1(a) and Fig. 1(b). Then, to comparatively evaluate the on-load DC winding induced voltage v_{load} in PS-WFSMs with

winding factors of even order harmonics $k_{2m}=0$ and $k_{2m}\neq 0$, the 12/10-pole PS-WFSMs with single layer AC windings shown in Fig. 1(c) in which $k_{2m}\neq 0$ is analyzed. Also, the 12/11-pole PS-WFSM with double layer AC windings is analyzed to investigate the influence of the relationship between harmonic orders of the open-circuit DC winding induced voltage v_{open} and the armature reaction DC winding induced voltage v_{arma} . They are summarized in TABLE I.

TABLE I

EVALUATION OF FOUR ANALYZED PS-WFSMs (DL=DOUBLE LAYER AND SL=SINGLE LAYER)

Evaluation	12/10 DL	6/4 DL	12/10 SL	12/11 DL
$LCM(N_s, N_r)=LCM(N_s/2, N_r)$?	No	Yes	No	No
$k_{2m}=0$?	Yes	No	No	Yes
v_{open} and v_{arma} have same harmonics orders?	Yes	Yes	No	No

A. Machine Optimization and Performance

The dimensional parameters of these analyzed PS-WFSMs are listed in TABLE II, which can be referred in Fig. 2. In TABLE II, the upper 9 parameters from l_s to l_{itb} are the same for all machines for a fair comparison. However, the lower 10 parameters from R_{osy} to θ_{it} in TABLE II are obtained by the global optimization. For each machine, the objective of the optimization is the same, i.e. the largest average electromagnetic torque, whilst the constrain is that the total copper loss $p_{cu}=120W$. As analyzed in [17], the average electromagnetic torque will achieve the highest value when the AC winding copper loss p_{cua} and the DC winding copper loss p_{cud} are equal. Therefore, they are designed to be the same during the optimization, i.e. $p_{cua}=p_{cud}=60W$. Since the rated rotor speed is low and hence the iron loss and PM eddy current loss are much smaller than the iron loss in the PS-WFSMs [17], they are not accounted in the optimization. ANSYS/Maxwell is chosen as the optimization tool. It is worth noting that all these machines operate in brushless AC (BLAC) model [18] with zero d -axis current control, i.e. $i_d=0$, due to negligible reluctance torque [17]. As for the 12/10-pole PS-WFSM with single layer AC windings shown in Fig. 1(d), it has the same dimensional parameters as its double layer counterpart shown in Fig. 1(a), but different AC winding topologies.

TABLE II

DIMENSIONAL PARAMETERS OF 12/10-, 12/11- AND 6/4-POLE PS-WFSMs WITH DOUBLE LAYER AC WINDINGS

Items	Unit	12/10	12/11	6/4
Stack length, l_s	mm	50	50	50
Outer radius of outer stator, R_{oso}	mm	45	45	45
Inner radius of inner stator, R_{isi}	mm	10.4	10.4	10.4
Length of outer (inner) air-gap, g_o (g_i)	mm	0.5	0.5	0.5
Length of outer stator tip top, l_{ott}	mm	0.5	0.5	0.5
Length of outer stator tip bottom, l_{otb}	mm	1.5	1.5	1.5
Length of inner stator tip top, l_{itt}	mm	0.5	0.5	0.5
Length of inner stator tip bottom, l_{itb}	mm	1.5	1.5	1.5
Yoke radius of outer stator, R_{osy}	mm	43	43	40.5
Inner radius of outer stator, R_{osi}	mm	36.5	36	34
Radius of rotor inner surface, R_{ri}	mm	33	33	29
Yoke radius of inner stator, R_{isy}	mm	12.5	12.5	15.5
Arc of outer stator tooth, θ_{ost}	°	6	6	11
Arc of outer stator tip, θ_{ot}	°	4	4	4
Arc of rotor piece outer edge, θ_{ro}	°	27	25	57
Arc of rotor piece inner edge, θ_{ri}	°	24	24	44
Arc of inner stator tooth, θ_{ist}	°	7	7	13
Arc of inner stator tip, θ_{it}	°	5	4	7

The open-circuit AC winding back-EMFs of the four analyzed PS-WFSMs are given in Fig. 3, in which N_{abc} is the number of turns per phase winding. As shown in Fig. 3(b), both the 6/4-pole PS-WFSM with double layer AC winding

and the 12/10-pole PS-WFSM with single layer AC winding suffer from even order harmonics, i.e. the winding factors of even order harmonics $k_{2m}\neq 0$. This leads to a high electromagnetic torque pulsating, as shown in Fig. 4. It is worth noting that in the analyzed machines AC coils belong to the same phase are connected in series.

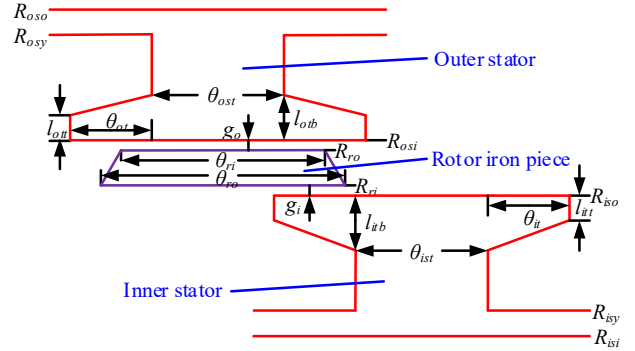


Fig. 2. Linear illustration of dimensional parameters in the PS-WFSM.

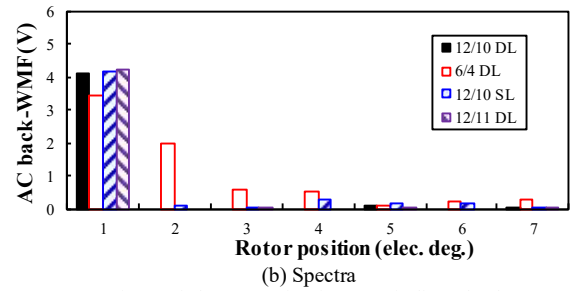
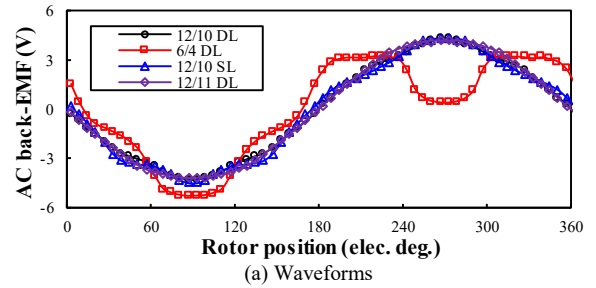


Fig. 3. Comparison of the open-circuit AC windings back-EMFs in four analyzed PS-WFSMs at 400rpm ($p_{cu}=60W$, $N_{abc}=72$).

The open-circuit AC winding back-EMFs shown in Fig. 3 and the electromagnetic torque shown in Fig. 4 are not relevant to the DC winding topology, if the wound field MMF per pole F_w is fixed. The influence of DC winding configuration on its induced voltage is investigated as follows, with consideration of conditions summarized in TABLE I.

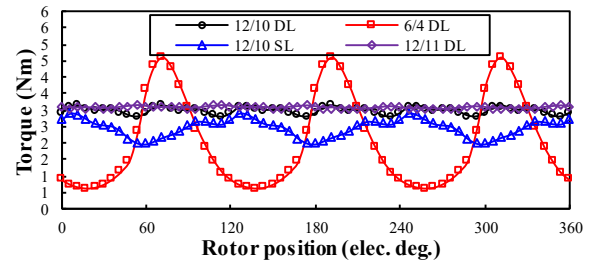


Fig. 4. Comparison of on-load electromagnetic torque waveforms in four analyzed PS-WFSMs at 400rpm ($p_{cua}=p_{cud}=60W$, BLAC, $i_d=0$).

B. Open-Circuit DC Winding Induced Voltage

As shown in Fig. 5, compared to the open-circuit induced voltage for DC coil W_{k+1} ($k=1, 2, 3 \dots N_w-1$), that for DC coil W_k lags $360^\circ N_r / LCM(N_w, N_r)$. As for the 12/10-pole PS-WFSM with double layer or single layer AC winding, since the open-circuit induced voltage for DC coil W_{k+6} ($k=1, 2, 3 \dots 6$) is exactly same as that for DC coil W_k . Therefore, the

maximum parallel branch number b_{max} for this case is 2. If $N_w=N_s/2=6$, the open-circuit induced voltages for DC coils W_{2k} ($k=1, 2, 3\dots 6$) are removed from Fig. 5, whilst those for DC coils W_{2k-1} are doubled due to the doubled coil turns. Again, the maximum parallel branch number $b_{max}=2$. Similar verification between the analytically predicted b_{max} shown in (12) and that from FE results in Fig. 5 can be conducted for the 6/4- and 12/11-pole PS-WFSMs.

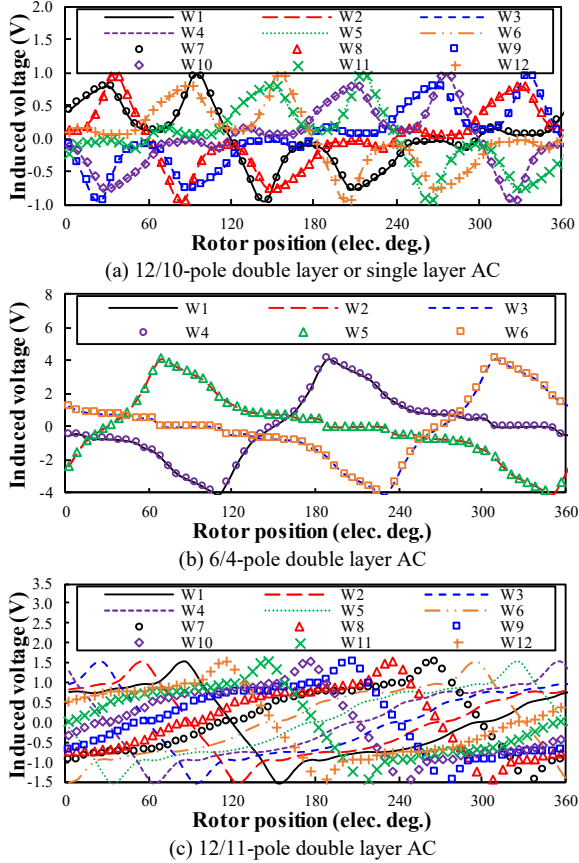


Fig. 5. Open-circuit DC coils induced voltages at 400rpm ($N_w=N_s$, $N_c N_w=1080$, $p_{cut}=60W$).

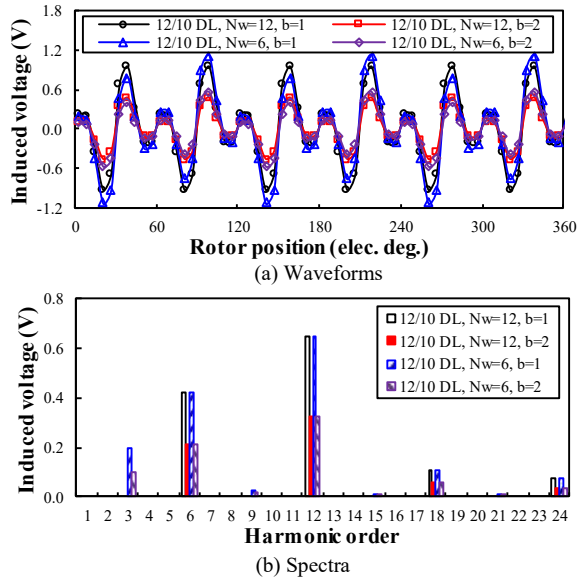


Fig. 6. Open-circuit DC winding induced voltages in the 12/10-pole PS-WFSM with double layer or single layer AC winding at 400rpm ($p_{cut}=60W$, $N_{abc}=72$).

As for the influence of the DC coil number N_w on the open-circuit DC winding induced voltage v_{open} , it is analyzed as follows. As shown in Fig. 6 and TABLE III, since $LCM(N_s, N_r) \neq LCM(N_s/2, N_r)$ for the 12/10-pole PS-WFSM with double layer or single layer AC winding, the

counterpart having $N_w=N_s/2=6$ suffers from more v_{open} harmonics, and hence a higher peak-to-peak value E_{ppopen} . Consequently, the open-circuit DC winding induced voltage ratio IVR_{open} is also higher in the counterpart having $N_w=N_s/2$, since the DC winding resistance voltage drop U_w is not relevant to the DC coil number N_w . Similar trend can be found for the 12/11-pole PS-WFSM, as shown in Fig. 7 and TABLE III. This means the open-circuit DC winding induced voltage v_{open} in the counterpart having $N_w=N_s/2$ challenges the DC power supply more and deteriorate the control performance more. This is consistent with the foregoing analytical analysis. However, as shown in Fig. 8 and TABLE III, since $LCM(N_s, N_r)=LCM(N_s/2, N_r)$ for the 6/4-pole PS-WFSM, all v_{open} harmonics, E_{ppopen} and IVR_{open} are the same for $N_w=N_s$ and $N_w=N_s/2$.

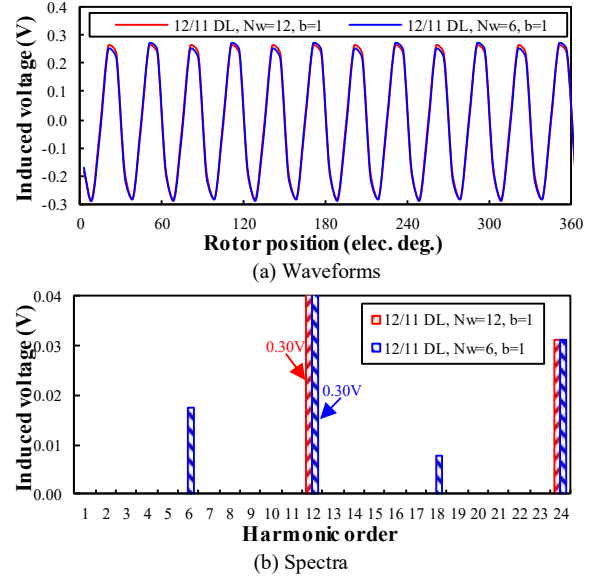


Fig. 7. Open-circuit DC winding induced voltages in the 12/11-pole PS-WFSMs with double layer AC winding at 400rpm ($p_{cut}=60W$, $N_{abc}=72$).

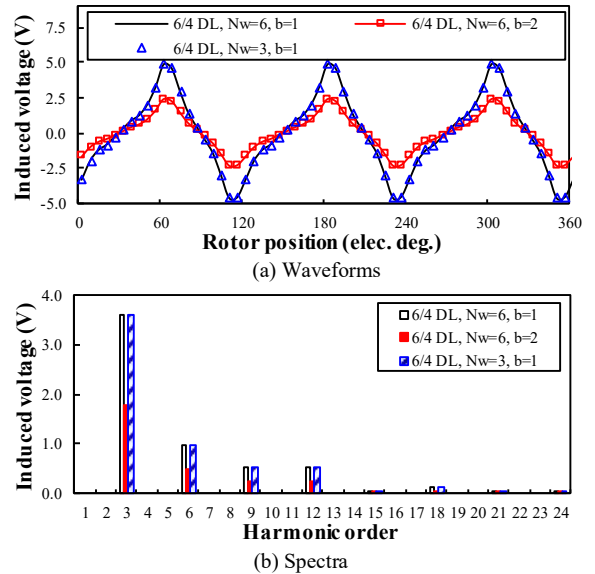


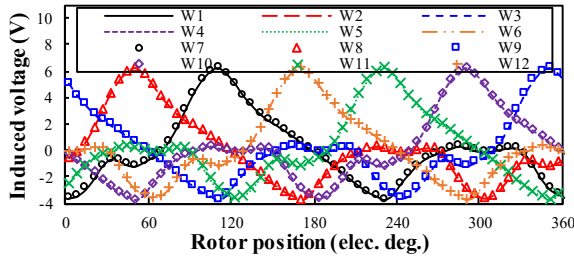
Fig. 8. Open-circuit DC winding induced voltages in the 6/4-pole PS-WFSMs with double layer AC winding at 400rpm ($p_{cut}=60W$, $N_{abc}=72$).

As for the influence of the parallel branch number b on the open-circuit DC winding induced voltage v_{open} , it is analyzed as follows. In all these four analyzed machines, same with the analytically predicted results, FE analysis also shows that the open-circuit DC winding induced voltage v_{open} and hence the peak-to-peak value E_{ppopen} are inversely proportional to the parallel branch number b , as shown in Fig. 6 - Fig. 8 and TABLE III. This means v_{open} and hence

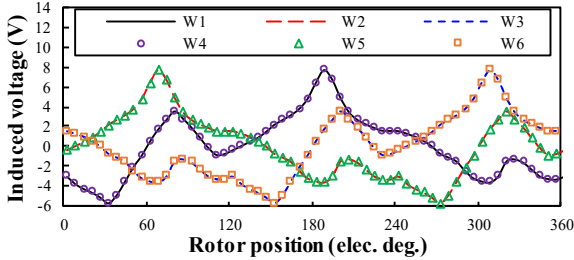
E_{ppopen} can be reduced by designing a higher parallel branch number b . However, since the DC winding resistance voltage drop U_w is also inversely proportional to the parallel branch number b , as shown in (4), the open-circuit DC winding induced voltage ratio IVR_{open} for various parallel branch number b are the same.

TABLE III
FE PREDICTED CHARACTERISTICS OF OPEN-CIRCUIT DC WINDING INDUCED VOLTAGES (HO=HARMONICS ORDERS, $k=1,2,3,\dots$)

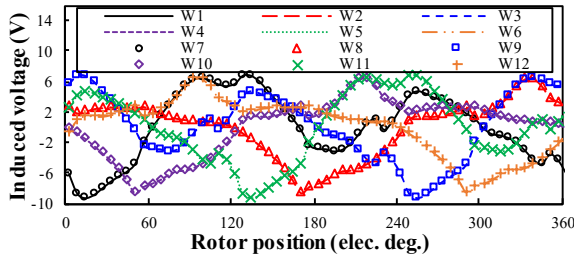
PS-WFSM	N_w	b	U_w (V)	E_{ppopen} (V)	IVR_{open} (%)	HO
12/10-pole double layer or single layer AC	12	1	16.47	1.89	11.45	$6k$
		2	8.24	0.94	11.45	$6k$
	6	1	16.47	2.49	15.11	$3k$
		2	8.24	1.25	15.11	$3k$
6/4-pole double layer AC	6	1	19.80	9.49	47.93	$3k$
		2	9.90	4.74	47.93	$3k$
	3	1	19.80	9.49	47.93	$3k$
12/11-pole double layer AC	12	1	16.41	0.54	3.29	$12k$
	6	1	16.41	0.55	3.37	$6k$



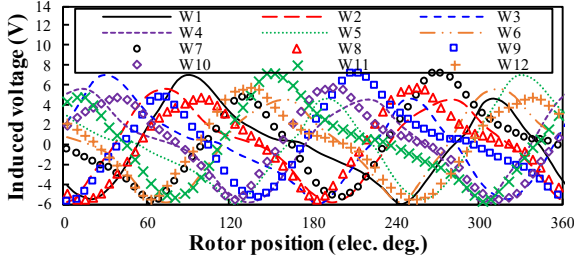
(a) 12/10-pole double layer AC



(b) 6/4-pole double layer AC



(c) 12/10-pole single layer AC



(d) 12/11-pole double layer AC

Fig. 9. On-load DC coil induced voltages 400rpm ($N_w=N_s$, $N_cN_w=1080$, $p_{cua}=p_{cuw}=60W$, BLAC, $i_d=0$).

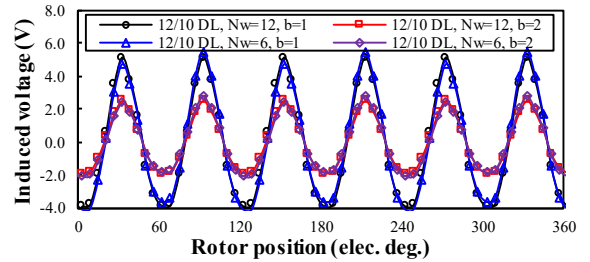
C. On-Load DC Winding Induced Voltage

The on-load DC winding induced voltage v_{load} of the four analyzed PS-WFSMs are shown in Fig. 9. As shown in Fig. 9(a) and Fig. 9(b), in the 12/10-pole PS-WFSM with double layer AC winding and 6/4-pole PS-WFSM, compared to the on-load DC winding induced voltage v_{load} for DC coil W_{k+1} ($k=1, 2, 3, \dots, N_w-1$), that for DC coil W_k lags $360^\circ N_r / LCM(N_w,$

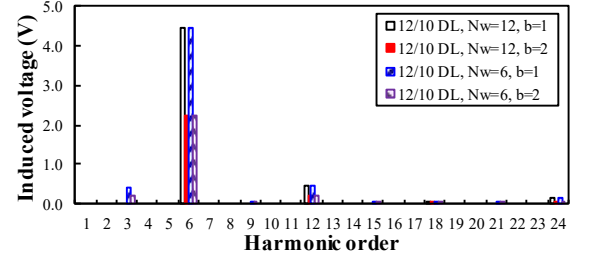
N_r). However, in the 12/10-pole PS-WFSM with single layer AC winding and 12/11-pole PS-WFSM, the on-load induced voltages for the adjacent two DC coils are distorted, as shown in Fig. 9(c) and Fig. 9(d).

TABLE IV
FE PREDICTED CHARACTERISTICS OF ON-LOAD DC WINDING INDUCED VOLTAGES (HO=HARMONICS ORDERS, $k=1,2,3,\dots$)

PS-WFSM	N_w	b	U_w (V)	E_{pload} (V)	IVR_{load} (%)	HO
12/10-pole double layer AC	12	1	16.47	8.95	54.31	$6k$
		2	8.24	4.47	54.31	$6k$
	6	1	16.47	9.74	59.12	$3k$
		2	8.24	4.87	59.12	$3k$
6/4-pole double layer AC	6	1	19.80	22.41	113.18	$3k$
		2	9.90	11.20	113.18	$3k$
	3	1	19.80	22.41	113.18	$3k$
12/10-pole single layer AC	12	1	16.47	24.08	146.16	$3k$
		2	8.24	12.04	146.16	$3k$
	6	1	16.47	24.45	148.39	$3k$
		2	8.24	12.22	148.39	$3k$
12/11-pole double layer AC	12	1	16.41	4.20	25.59	$6k$
	6	1	16.41	4.29	26.12	$6k$

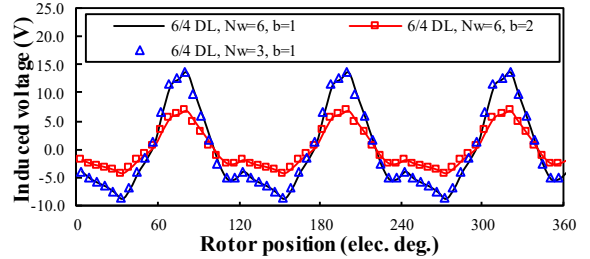


(a) Waveforms

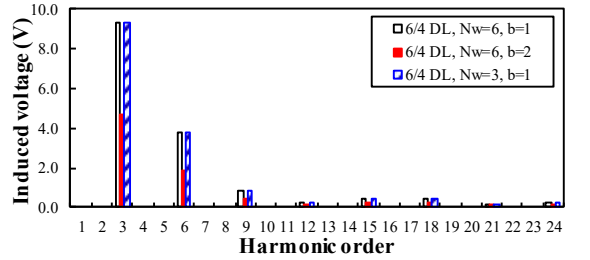


(b) Spectra

Fig. 10. On-load DC winding induced voltages in the 12/10-pole PS-WFSM with double layer AC winding at 400rpm ($N_cN_w=1080$, $p_{cua}=p_{cuw}=60W$).



(a) Waveforms



(b) Spectra

Fig. 11. On-load DC winding induced voltages in the 6/4-pole PS-WFSM with double layer AC winding at 400rpm ($N_cN_w=1080$, $p_{cua}=p_{cuw}=60W$).

On-load DC winding induced voltages in the four analyzed PS-WFSMs with different DC winding configurations are shown in Fig. 10 - Fig. 13, of which the characteristics are summarized in TABLE IV. As shown in

TABLE III and TABLE IV, in the 12/10-pole PS-WFSM with double layer AC winding and 6/4-pole PS-WFSM, the harmonic orders for the on-load and the open-circuit DC winding induced voltages for various DC coil number N_w and parallel branch number b are the same, respectively. However, for the 12/11-pole PS-WFSM having $N_w=N_s=12$ and $b=1$, the harmonic orders for the on-load DC winding induced voltage v_{load} is $6k$ ($k=1,2,3\dots$) whilst those for the open-circuit DC winding induced voltage v_{open} is $12k$. This is due to the harmonic orders for the armature reaction DC winding induced voltage v_{arma} are $6k$.

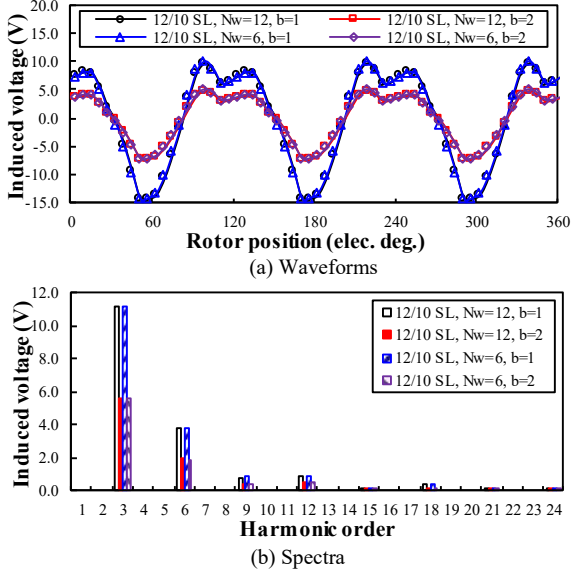


Fig. 12. On-load DC winding induced voltages in the 12/10-pole PS-WFSM with single layer AC winding at 400rpm ($N_c N_w=1080$, $p_{cu}=p_{cu}=60W$).

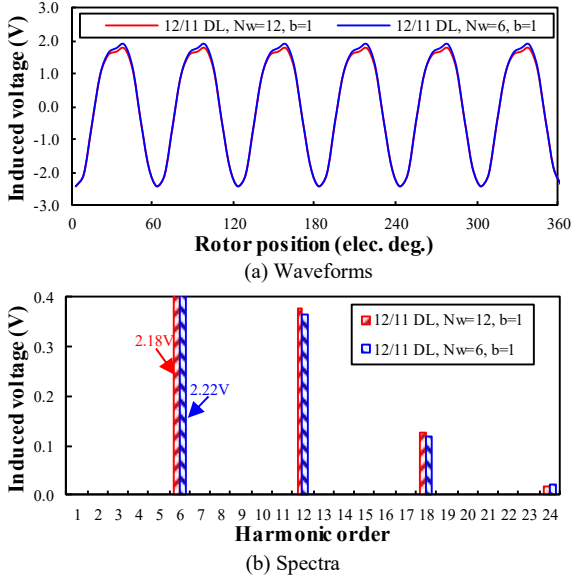


Fig. 13. On-load DC winding induced voltages in the 12/11-pole PS-WFSM with double layer AC winding at 400rpm ($N_c N_w=1080$, $p_{cu}=p_{cu}=60W$).

Moreover, as shown in TABLE IV and Fig. 12, for the 12/10-pole PS-WFSM with single layer AC winding having $N_w=N_s=12$, harmonic orders for the on-load DC winding induced voltage v_{load} are $3k$, different from that with double layer AC winding, i.e. $6k$. The reason is that the winding factors of even order harmonics $k_{2m} \neq 0$, which is evidenced by Fig. 3. Due to more harmonics, the on-load DC winding induced voltage v_{load} in 12/10-pole PS-WFSM with single layer AC winding and hence the peak-to-peak value E_{pload} and the on-load DC winding induced voltage ratio IVR_{load} are higher than its counterpart with double layer AC winding. This means the on-load DC winding induced voltage in the

counterpart with single layer AC winding may cause significant challenge for the DC power supply and deteriorate the control performance. This is consistent with the foregoing analytical analysis.

By comparing the open-circuit DC winding induced voltage v_{open} and the on-load DC winding induced voltage v_{load} in TABLE III, TABLE IV and Fig. 5 - Fig. 13, two conclusions can be obtained. Firstly, PS-WFSMs feature non-zero winding factors for even order harmonics, i.e. $k_{2m} \neq 0$, suffer from a higher DC winding induced voltage ratio IVR and hence a challenged control performance. Secondly, more harmonic orders also indicate higher IVR .

VI. EXPERIMENTAL VALIDATION

To validate the foregoing analytical and FE analyses, the 12/10-pole PS-WFSM having double layer AC winding with $N_w=N_s$ and $b=1$ is built and tested, as shown in Fig. 14. To validate the FE predicted DC winding induced voltages under constant DC currents, the current source is used as the power supply for DC winding. It is worth noting that in the prototype a 0.5mm thick rotor iron bridge is introduced adjacent to the inner air-gap to connect the rotor iron pieces. This is for easing assembling of the laminations of the rotor iron pieces and hence easing manufacturing of the cup rotor shown in Fig. 14(b).

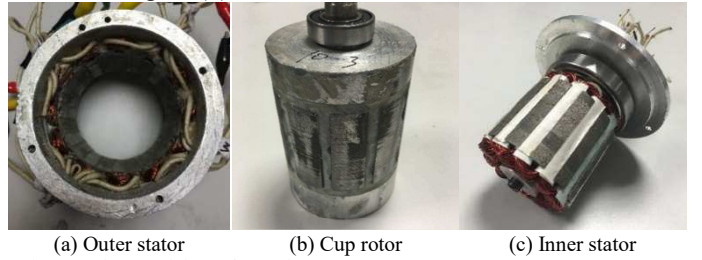


Fig. 14. Photos of the 12/10-pole PS-WFSM prototype.

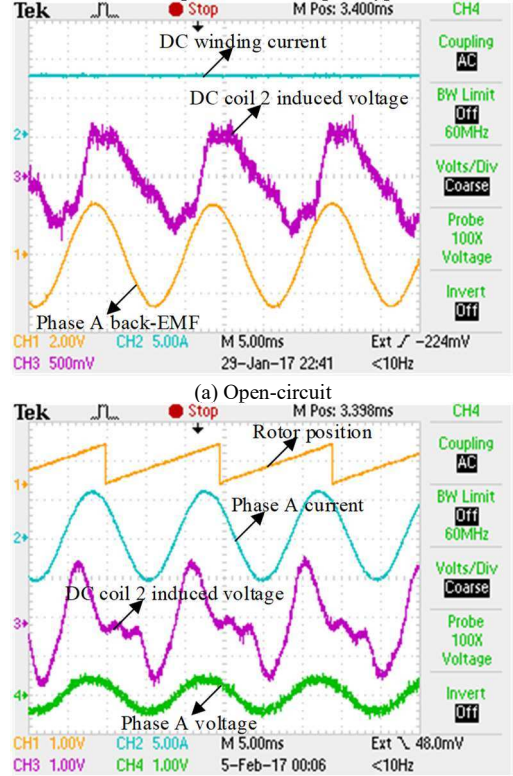


Fig. 15. Measured open-circuit phase A back-EMF, open-circuit and on-load DC coil 2 induced voltages at 400rpm.

The measured open-circuit phase A back-EMF, open-

circuit and on-load DC coil 2 induced voltages at 400rpm are shown in Fig. 15. As shown in Fig. 16, the measured results in Fig. 15 agree well with the 2-D FE predicted values, in which the lamination stacking factor is 0.9. This trend can also be observed from Fig. 17 for the static torques. It is worth noting that the prototype operates in generator mode connected with three-phase symmetrical pure resistance load $R_{load}=0.1\Omega$ for Fig. 15(b).

It is worth noting that since the impact of the DC power supply on the induced voltage cannot be separated, it is not the entire DC winding induced voltage but that of the DC coil 2, which is open-circuited with DC coils 4, 6, 8, 10 and 12, that is measured. However, DC coils 1, 3, 5, 7, 9 and 11 are loaded with $2I_w=7.2A$ to generate the same F_w as would be the case if all DC coils were loaded with $I_w=3.6A$.

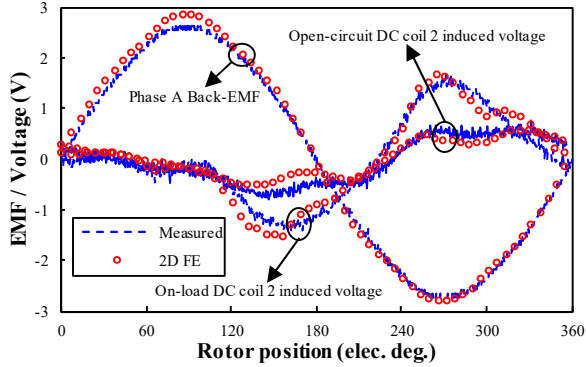


Fig. 16. Comparison between the measured and FE predicted open-circuit phase A back-EMFs and DC coil 2 induced voltages at 400rpm.

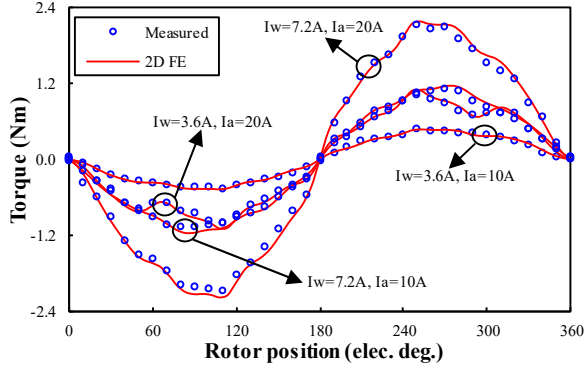


Fig. 17. Comparison between the measured and FE predicted static torques ($I_a=-2I_b=-2I_c$).

TABLE V

KEY SPECIFICATIONS OF THE 12/10-POLE PS-WFSM PROTOTYPE (EXP=EXPERIMENT, WI/WO=WITH/WITHOUT IRON BRIDGE)

Items	Unit	Exp	Wi	FE	Wi	FE	Wo
Rated speed, Ω_r	rpm	400	400	400			
Rated torque when $p_{cu}=120W$, T_r	Nm	2.06	2.25	2.67			
Rated power when $p_{cu}=120W$, P_r	W	86.29	94.25	111.97			
Rated open-circuit AC winding phase fundamental back-EMF, E_{ph1}	V	2.63	2.75	3.70			
Rated open-circuit DC winding induced voltage peak-to-peak, E_{ppopen}	V	1.07	1.56	1.70			
On-load DC winding induced voltage peak-to-peak with $R_{load}=0.1\Omega$, E_{ppload}	V	3.09	3.19	8.06			

The tested key specifications of the 12/10-pole PS-WFSM prototype with iron bridge and those predicted by 2-D FE are shown in TABLE V, together with those of its counterpart without iron bridge predicted by 2-D FE. Due to the introduction of the iron bridge and hence the flux leakage, the open-circuit AC winding phase fundamental back-EMF E_{ph1} is reduced by 34.51%, i.e. 3.70V and 2.75V, respectively. However, due to a more saturated iron bridge and hence a smaller leakage permeance, the rated average electromagnetic torque and hence power with iron bridge is only 18.8% smaller.

VII. IMPACT OF DC WINDING INDUCED VOLTAGE

In WFSMs, the DC winding excitation can be realized by using a current source shown in Fig. 18(a), a voltage source converter with a half H-bridge shown in Fig. 18(b), or a full H-bridge shown in Fig. 18(c), respectively. Take the rated on-load condition of the 12/10-pole PS-WFSM having single layer AC winding of which the rated DC winding current $I_w=3.64A$ and the corresponding DC resistance voltage drop $U_w=16.5V$ as example, the impact of DC winding induced voltage is explained as follows.

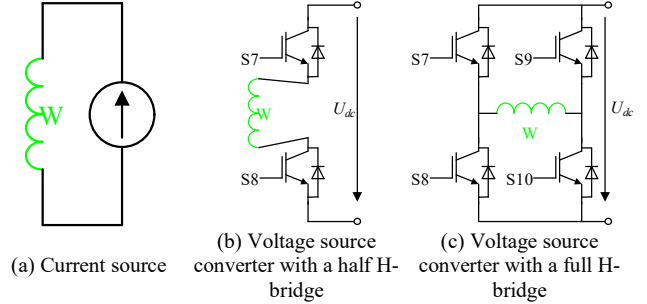


Fig. 18. DC winding drive circuits for WFSMs.

A. Current Source

As for the WFSMs in which DC winding is supplied by the current source, the challenge caused by the DC winding induced voltage is mainly from three aspects.

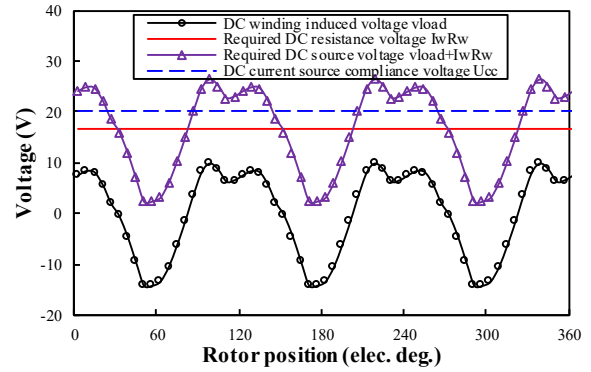


Fig. 19. Rated on-load DC winding induced voltage, required DC resistance voltage (16.47V), required DC source voltage, and the DC source compliance voltage waveforms for the 12/10-pole PS-WFSM having single layer AC winding at 400rpm ($p_{cu}=p_{cu1}=60W$, BLAC, $i_d=0$).

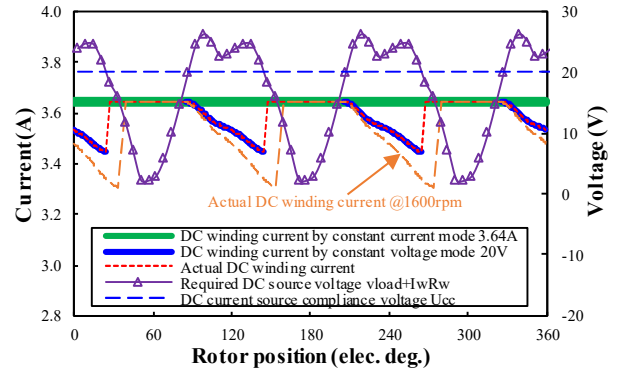


Fig. 20. Rated on-load DC winding current of the 12/10-pole PS-WFSM having single layer AC winding at 400rpm (Current source output is 3.64A, of which the compliance voltage is 20V, $p_{cu}=p_{cu1}=60W$, BLAC, $i_d=0$).

Firstly, if the compliance voltage of the DC current source is $U_{dcc}=20V$, it will be smaller than the required DC source voltage within some rotor position ranges, i.e. $U_{dcc}<v_{load}+I_wR_w$, as shown in Fig. 19. This means the DC power supply will abruptly stop being a current source when the machine operates at these rotor positions. For some commercial DC power supplies, they will switch from constant current mode to constant voltage mode with an

output voltage $U_{dc}=20V$. Assuming that the switch between current mode and voltage mode for the current source is instantaneous, the resulted DC winding current by constant voltage mode in these rotor position ranges can be shown as the blue solid line in Fig. 20. Therefore, the actual DC winding current is shown in Fig. 20 as the red dash line. Compared with the constant DC winding current $I_w=3.64A$, the actual DC winding current will be smaller in three rotor position ranges, due to the DC winding induced voltage. The DC winding current will reduce more in wider rotor position ranges at a higher speed, e.g. the actual DC winding current of the machine at 1600rpm shown in Fig. 20.

Secondly, if the on-load DC winding induced voltage v_{load} is even higher than the compliance voltage U_{dc} at a high rotor speed, i.e. $v_{load} > U_{dc}$, the current source is risky to suffer from a reverse input current.

Thirdly, the current source will also suffer from a reverse voltage at a high rotor speed due to the DC winding induced voltage negative value. This may activate the reverse voltage protection in the current source.

B. Voltage Source Converter with Half or Full H-Bridge

For this case, the closed-loop current control is usually implemented to achieve a stable current in the DC winding. As shown in Fig. 21(a), when the on-load DC winding induced voltage v_{load} is neglected, the DC winding excitation circuit is usually modelled as a first-order impedance circuit with resistance R_w and average self-inductance L_{w0} .

However, a more stable DC winding current i_w can be obtained if the DC winding induced voltage v_{load} is considered as a disturbed voltage, as shown in Fig. 21(b). Here, a higher DC winding bus voltage U_{dc} shown in Fig. 18(b) is required to balance the DC winding induced voltage v_{load} . Since the on-load DC winding induced voltage v_{load} is proportional to the rotor speed, the DC winding bus voltage U_{dc} needs to be higher at a larger rotor speed. This means the rotor speed will be limited for a certain DC winding bus voltage U_{dc} , due to the existence of DC winding induced voltage. On the other hand, a reverse output voltage from converter may be required to balance the DC winding induced voltage negative value at high speed. Since the half H-bridge cannot achieve this function, only the full H-bridge with a higher cost can be adopted.

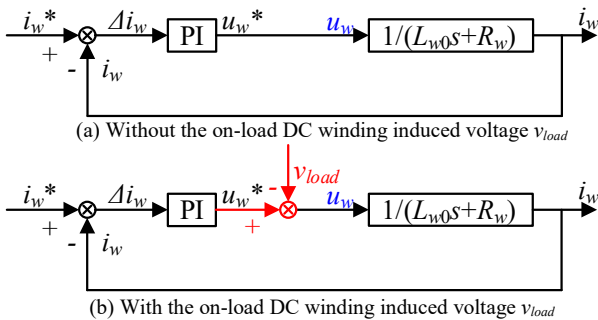


Fig. 21. Control diagram for DC winding current without and with consideration of the on-load DC winding induced voltage v_{load} .

VIII. CONCLUSION

In this paper, the influence of DC winding configuration including the DC coil number N_w and parallel branch number b on DC winding induced voltage pulsation in WFSM machines is investigated. The DC winding configuration design is restricted due to its induced voltage pulsation. The feasible and preferred DC winding configuration for various stator/rotor-pole combinations with double layer or single

layer AC windings are obtained. The following design recommendations for WFSMs are made:

- 1) In WFSMs with $LCM(N_s, N_r) \neq LCM(N_s/2, N_r)$, it is recommended to design $N_w=N_s$ but not $N_w=N_s/2$, for a smaller open-circuit DC winding induced voltage ratio IVR_{open} . However, in WFSMs with $LCM(N_s, N_r)=LCM(N_s/2, N_r)$, both $N_w=N_s$ and $N_w=N_s/2$ are feasible.
- 2) Although a higher DC winding parallel branch number b can decrease the DC power supply voltage, it is not free to design but with a maximum feasible value $b_{max}=N_w N_r / LCM(N_w, N_r)$, due to the different induced voltages among DC coils. Otherwise, circulating currents among DC coils will be generated, increasing the copper loss and decreasing the efficiency.
- 3) WFSMs having non-zero winding factors of even orders harmonics, i.e. $k_{2m} \neq 0$, are not recommended due to the higher on-load DC winding induced voltage v_{load} caused by the $3k^{th}$ ($k=1,2,3\dots$) harmonics, which will challenge the DC power supply more and deteriorate the control performance more.

APPENDIX A

The open-circuit induced voltage v_k for the DC coil W_k can be expressed as,

$$v_{k_open}(\theta_e) = \sum_{j=1}^{\infty} N_c M_j \Omega \sin[j(\theta_e - \beta_k) + \alpha_j] \quad (A.1)$$

where $N_c M_j \Omega$ and α_j are the amplitude and initial phase for the j^{th} harmonic, respectively. θ_e is the rotor electric position. M_j is the j^{th} amplitude of the open-circuit induced voltage for each turn in the DC coil per rotor mechanical speed unit. It is worth noting that M_j and α_j are the same in a certain WFSM with same magnetic field having different DC winding configurations. Ω is the rotor mechanical speed. β_k is the fundamental electric lag angle between the DC coil W_k and W_1 , which can be given by,

$$\beta_k = \frac{2(k-1)\pi N_r}{N_w} \quad (A.2)$$

Accounting for the parallel branch number b , the open-circuit DC winding induced voltage v_{open} can be given by,

$$v_{open}(\theta_e) = \frac{1}{b} \sum_{k=1}^{N_w} v_{k_open}(\theta_e) \quad (A.3)$$

Submitting (A.1) and (A.2) to (A.3), v_{open} can be rewritten as,

$$v_{open}(\theta_e) = \frac{N_c \Omega}{b} \sum_{j=1}^{\infty} M_j \sum_{k=1}^{N_w} \sin(pk + q) \quad (A.4)$$

where

$$p = -\frac{2j\pi N_r}{N_w} \quad (A.5)$$

and

$$q = j\theta_e + \frac{2j\pi N_r}{N_w} + \alpha_j \quad (A.6)$$

v_{open} in (A.4) can be simplified as,

$$v_{open}(\theta_e) = \frac{N_c \Omega}{b} \sum_{j=1}^{\infty} M_j \left[\cos q \sum_{k=1}^{N_w} \sin pk + \sin q \sum_{k=1}^{N_w} \cos pk \right] \quad (A.7)$$

Since

$$\sum_{k=1}^{N_w} \sin pk = \frac{\sin \frac{N_w p}{2}}{\sin \frac{p}{2}} \sin \frac{(N_w + 1)p}{2} \quad (\text{A. 8})$$

and

$$\sum_{k=1}^{N_w} \cos pk = \frac{\sin \frac{N_w p}{2}}{\sin \frac{p}{2}} \cos \frac{(N_w + 1)p}{2} \quad (\text{A. 9})$$

therefore,

$$v_{open}(\theta_e) = \frac{N_c \Omega}{b} \sum_{j=1}^{\infty} M_j \frac{\sin \frac{N_w p}{2}}{\sin \frac{p}{2}} \sin \left[q + \frac{(N_w + 1)p}{2} \right] \quad (\text{A. 10})$$

Submitting (A. 5) and (A. 6) to (A. 10), v_{open} can be expressed as,

$$v_{open}(\theta_e) = \frac{N_c \Omega}{b} \sum_{j=1}^{\infty} M_j \frac{\sin j N_r \pi}{\sin \frac{j N_r \pi}{N_w}} \sin \left(j \theta_e + \frac{j \pi N_r}{N_w} + \alpha_j - j \pi N_r \right) \quad (\text{A. 11})$$

As can be seen from (A. 11), $v_{open}=0$ unless $\sin(j N_r \pi / N_w) \neq 0$, i.e. $j N_r / N_w$ is an integer. Here,

$$\lim_{\substack{j N_r \pi \rightarrow 0 \\ \sin \frac{j N_r \pi}{N_w}}} \frac{\sin j N_r \pi}{\sin \frac{j N_r \pi}{N_w}} = \frac{\cos j N_r \pi}{\cos \frac{j N_r \pi}{N_w}} N_w = \pm N_w \quad (\text{A. 12})$$

Since $j N_r / N_w$ is an integer, j can be given by,

$$j = m \frac{\text{LCM}(N_w, N_r)}{N_r} \quad (\text{A. 13})$$

where LCM is the least common multiplier and $m=1,2,3\dots$

Based on (A. 11), (A. 12) and (A. 13), v_{open} can be rewritten as (6).

APPENDIX B

The armature reaction DC winding flux-linkage ψ_{arma} can be expressed as,

$$\psi_{arma}(\theta_e) = \frac{N_w N_c}{b} M_{wa}(\theta_e) i_a(\theta_e) + \frac{N_w N_c}{b} M_{wb}(\theta_e) i_b(\theta_e) + \frac{N_w N_c}{b} M_{wc}(\theta_e) i_c(\theta_e) \quad (\text{B. 1})$$

where $N_w N_c M_{wa} / b$, $N_w N_c M_{wb} / b$ and $N_w N_c M_{wc} / b$ are the mutual inductance between the A-, B- and C-phase windings and DC winding, respectively. M_{wa} , M_{wb} and M_{wc} can be given as Fourier series as,

$$\begin{cases} M_{wa}(\theta_e) = \sum_{j=1,2,3,\dots}^{\infty} p_j d_j M_j \cos(j \theta_e + \delta_j) \\ M_{wb}(\theta_e) = \sum_{j=1,2,3,\dots}^{\infty} p_j d_j M_j \cos \left[j \left(\theta_e - \frac{2}{3} \pi \right) + \delta_j \right] \\ M_{wc}(\theta_e) = \sum_{j=1,2,3,\dots}^{\infty} p_j d_j M_j \cos \left[j \left(\theta_e + \frac{2}{3} \pi \right) + \delta_j \right] \end{cases} \quad (\text{B. 2})$$

where $p_j d_j M_j$ and δ_j are the amplitude and initial phase of the j^{th} mutual-inductance harmonic. p_j and d_j are the j^{th} harmonic pitch factor and distribution factor of the windings, respectively, [17].

The 3-phase symmetrical sinusoidal phase currents i_a , i_b and i_c can be given by,

$$\begin{cases} i_a = I_1 \cos(\theta_e + \sigma_1) \\ i_b = I_1 \cos(\theta_e + \sigma_1 - \frac{2}{3} \pi) \\ i_c = I_1 \cos(\theta_e + \sigma_1 + \frac{2}{3} \pi) \end{cases} \quad (\text{B. 4})$$

where I_1 and γ_1 are the fundamental amplitude and initial phase, respectively.

Based on (B. 1), (B. 2) and (B. 4), the DC winding voltage induced by armature reaction v_{arma} can be rewritten as (15).

REFERENCES

- [1] A. M. El-Refai, T. M. Jahns, and D. W. Novotny, "Analysis of surface permanent magnet machines with fractional-slot concentrated windings," *IEEE Trans. Energy Convers.*, vol. 21, no. 1, pp. 34-43, Mar. 2006.
- [2] J. Cros, and P. Viarouge, "Synthesis of high performance PM motors with non-overlapping windings," *IEEE Trans. Energy Convers.*, vol. 17, no. 2, pp. 248-253, Jun. 2002.
- [3] I. Boldea, L. N. Tutelea, L. Parsa, and D. Dorrell, "Automotive electric propulsion systems with reduced or no permanent magnets: an overview," *IEEE Trans. Ind. Electron.*, vol. 61, no. 10, pp. 5696-5711, Oct. 2014.
- [4] M. L. Bash, and S. D. Pekarek, "Modeling of salient-pole wound-rotor synchronous machines for population-based design," *IEEE Trans. Energy Convers.*, vol. 26, no. 2, pp. 381-392, Jun. 2011.
- [5] Z. Zhang, Y. Yan, and Y. Tao, "A new topology of low speed doubly salient brushless DC generator for wind power generation," *IEEE Trans. Magn.*, vol. 48, no. 3, pp. 1227-1233, Mar. 2012.
- [6] J. T. Chen, Z. Q. Zhu, S. Iwasaki, and R. Deodhar, "Low cost flux-switching brushless AC machines," *Proc. Conf. Veh. Pow. Prop.*, Lille, France, 2010, pp. 1-6.
- [7] C. Pollock and M. Wallace, "The flux switching motor, a DC motor without magnets or brushes," in *Conf. Rec. IEEE IAS Annu. Meeting*, 1999, vol. 3, pp. 1980-1987.
- [8] C. Yu, and S. Niu, "Development of a magnetless flux switching machine for rooftop wind power generation," *IEEE Trans. Energy Convers.*, vol. 30, no. 4, pp. 1703-1711, Dec. 2015.
- [9] A. Zulu, B. Mecrow, and A. Armstrong, "A wound-field three-phase flux switching synchronous motor with all excitation sources on the stator," *IEEE Trans. Ind. Appl.*, vol. 46, no. 6, pp. 2363-2371, Nov.-Dec. 2010.
- [10] Y. Tang, J. J. H. Paulides, T. E. Motoasca, and E. A. Lomonova, "Flux switching machine with DC excitation," *IEEE Trans. Magn.*, vol. 48, no. 11, pp. 3583-3586, Nov. 2012.
- [11] E. Sulaiman, T. Kosaka, and N. Matsui, "A new structure of 12 slot-10 pole field-excitation flux switching synchronous machine for hybrid electric vehicles," in *Proc. 14th Eur. Conf. Power Electron. Appl.*, Birmingham, UK, Aug.-Sep. 2011, pp. 1-10, paper 245.
- [12] E. Sulaiman, T. Kosaka, and N. Matsui, "Design study and experimental analysis of wound field flux switching motor for HEV applications," in *Proc. IEEE Inter. Conf. Elec. Mach.*, Marseille, France, Sep. 2012, pp. 1269-1275.
- [13] T. Raminosoa, A. M. El-Refai, D. Pan, K. K. Huh, J. P. Alexander, K. Grace, S. Grubic, S. Galioto, P. B. Reddy, and X. Shen, "Reduced rare-earth flux-switching machines for traction applications," *IEEE Trans. Ind. Appl.*, vol. 51, no. 4, pp. 2959-2971, Jul.-Aug. 2015.
- [14] T. Raminosoa, D. Torrey, A. M. El-Refai, K. Grace, D. Pan, S. Grubic, K. Bodla, and K.-K. Huh, "Sinusoidal reluctance machine with DC winding: an attractive non-permanent magnet option," in *Proc. IEEE Energy Convers. Congr. Expo.*, Montreal, QC, Canada, Sep. 2015, pp. 310-317.
- [15] B. Fahimi, A. Emadi, and R. B. Sepe, "A switched reluctance machine-based starter/alternator for more electric cars," *IEEE Trans. Energy Convers.*, vol. 19, no. 1, pp. 116-124, Mar. 2004.
- [16] A. Chiba, Y. Takano, M. Takeno, T. Imakawa, N. Hoshi, M. Takemoto, and S. Ogasawara, "Torque density and efficiency improvements of a switched reluctance motor without rare-earth material for hybrid vehicles," *IEEE Trans. Ind. Appl.*, vol. 47, no. 3, pp. 1240-1246, May-Jun. 2011.
- [17] Z. Q. Zhu, Z. Z. Wu, D. J. Evans, and W. Q. Chu, "A wound field switched flux machine with field and armature windings separately wound in double stators," *IEEE Trans. Energy Convers.*, vol. 30, no. 2, pp. 772-783, Jun. 2015.
- [18] W. L. Soong, and T. J. E. Miller, "Field-weakening performance of brushless synchronous AC motor drives," *IEE Proc. Elec. Power Appl.*, vol. 141, no. 6, pp. 331-340, Nov. 1994.



Z. Z. Wu (S'15-M'18) received the B.Eng. and M.Eng. degrees in electrical engineering from Southeast University, Nanjing, China, in 2010 and 2013, respectively, and the Ph.D. degree in electrical and electronic engineering from The University of Sheffield, Sheffield, U.K., in January 2017.

Since January 2017, he has been with Warwick Manufacturing Group (WMG), The University of Warwick, Coventry, U.K., where he is currently a research fellow. His major research interests

include the analysis, design, control and manufacturing of synchronous machines and magnetic gear for electrical vehicle and wind power generation applications.



P. Farah received the Ph.D. degree in electrical engineering from the Institute National Polytechnique de Grenoble, France, in 1995.

From 2013 to 2016, he was with Valeo Engine and Electrical Systems, Creteil, France, as the Director of the Electromagnetic Design Group.



Z. Q. Zhu (M'90–SM'00–F'09) received the B.Eng. and M.Sc. degrees in electrical and electronic engineering from Zhejiang University, Hangzhou, China, in 1982 and 1984, respectively, and the Ph.D. degree in electrical and electronic engineering from The University of Sheffield, Sheffield, U.K., in 1991.

Since 1988, he has been with The University of Sheffield, where he is currently a Research Chair of the Royal Academy of Engineering/Siemens with the

Department of Electronic and Electrical Engineering and the Head of the Electrical Machines and Drives Research Group. His current major research interests include the design and control of permanent-magnet brushless machines and drives for applications ranging from automotive through domestic appliance to renewable energy. He is a Fellow of the Royal Academy of Engineering.



C. Wang received the B.Eng. and M.Sc. degrees in electrical engineering from Hefei University of Technology, Hefei, China, in 2008 and 2011, respectively. He is currently working toward the Ph.D. degree in electronic and electrical engineering from the University of Sheffield, Sheffield, U.K.

From 2011 to 2015, he was an Engineer at Midea Welling Motor Technology Company, Ltd., Shanghai, China. His research interests include the

control of electric drives.



J. C. Mipo received the Ph.D. degree in electrical engineering from Pierre-and-Marie-Curie University, Paris, France, in 1998.

Since 1998, he has been with Valeo Engine and Electrical Systems, Creteil, France, where he is currently an Advanced Technical Manager.



S. Personnaz received the Ph.D. degree in electric engineering from the Laboratoire d'Electrotechnique de Grenoble, Grenoble, France, in 1992.

Since 2017, she has been with Valeo Engine and Electrical Systems, Creteil, France, where she is currently the PES Electrotechnical Director, one of Powertrain Electrical System core activity. She leads the team of electric machine

designers for the low voltage applications.